Research Paper

Tumour-homing chimeric polypeptide-conjugated polypyrrole nanoparticles for imaging-guided synergistic photothermal and chemical therapy of cancer

Mengmeng Sun[1], Jianwen Guo[1], Hanjun Hao[1], Tong Tong[2], Kun Wang[2] and Weiping Gao[1✉]

1. Department of Biomedical Engineering, School of Medicine, Tsinghua University, Beijing 100084, China
2. Key Laboratory of Molecular Imaging, the State Key Laboratory of Management and Control for Complex Systems, Institute of Automation, Chinese Academy of Sciences, Beijing, 100190, China.

✉ Corresponding author: gaoweiping@tsinghua.edu.cn

Abstract

Near-infrared (NIR)-absorbing conjugated polymer nanoparticles are interesting for imaging-guided combination therapy, especially for synergistic photothermal therapy and chemotherapy; however, most of them target tumours passively through the enhanced permeability and retention (EPR) effect, leading to low utilization efficiency. To address this problem, we report an active tumour-targeting strategy of tumour-homing chimeric polypeptide-conjugated NIR-absorbing conjugated-polymer nanoparticles as a new class of drug nanocarriers for imaging-guided combination therapy of cancer.

Methods: A tumour-homing chimeric polypeptide C-ELP-F3 was genetically engineered, and chemoselectively conjugated to polypyrrole (PPy) nanoparticles via a facile thiol-maleimide coupling reaction to form ELP-F3 conjugated PPy (PPy-ELP-F3) nanoparticles. Doxorubicin (DOX) was physically adsorbed onto PPy-ELP-F3 nanoparticles to yield DOX-loaded PPy-ELP-F3 (DOX/PPy-ELP-F3) nanoparticles. The physicochemical properties of DOX/PPy-ELP-F3 were characterized. The pharmacokinetics of DOX/PPy-ELP-F3 was studied in a mouse model. The photoacoustic imaging and photothermal imaging of tumours were tested in a melanoma-bearing mouse model. The photothermal-chemical combination therapy of tumours was investigated by using melanoma cells *in vitro* and in a melanoma-bearing mouse model.

Results: DOX/PPy-ELP-F3 nanoparticles showed enhanced cytotoxicity to melanoma cells *in vitro* and improved tumour-targeting efficiency *in vivo*, as compared with both DOX/PPy-ELP nanoparticles without the tumour-homing function and free DOX. The photothermal effect of DOX/PPy-ELP-F3 nanoparticles could accelerate the release of DOX from PPy-ELP-F3. Under the guidance of photoacoustic and photothermal imaging, the synergy of photothermal and chemical therapy could completely abolish tumours without detectable systemic toxicity.

Conclusion: Tumour-homing chimeric polypeptide-conjugated NIR-absorbing conjugated-polymer nanoparticles are promising as a new multifunctional drug delivery platform for highly-efficient imaging guided combination therapy.

Key words: tumour targeting; nanomedicine; polypyrrole; photothermal therapy; combination therapy

Introduction

Near infrared (NIR) light can be focused on a specific region with easy operation, and can noninvasively penetrate into reasonably deep tissues due to its minimal absorbance by skin and tissues [1]. These characteristics of NIR light render NIR-absorbing photothermal agents crucial for

photothermal therapy in which NIR light can be absorbed and transformed into heat efficiently to ablate cancer cells [2-8]. NIR-absorbing organic nanomaterials are generally less toxic and more biocompatible than inorganic ones [9,10], so several NIR-absorbing conjugated polymers, such as polypyrrole (PPy) [11-15], polyaniline [16] and poly(3,4-ethylenedioxythiophene):poly(4-styre-nesulf onate) (PEDOT:PSS) [17] have recently attracted much attention as a new class of photothermal agents for cancer therapy. Furthermore, conjugated polymer nanoparticles have been explored as drug carriers for combined photothermal and chemical/photo-dynamic/radioisotope therapy of cancer [18-23]. Drugs such as doxorubicin (DOX) and porphyrin can be loaded into these conjugated polymer nanoparticles through π-π stacking. The photothermal effect of the conjugated polymer nanoparticles can be used to not only directly kill cancer cells by hyperthermia, but also trigger the on-demand release of drugs from the nanoparticles or enhance the cellular uptake of drugs loaded in the nanocarriers to significantly improve the efficacy of chemical or photodynamic therapy.

These conjugated polymer nanoparticles usually accumulate in the tumour via the enhanced permeability and retention (EPR) effect [11,12,14-20,22]. However, the passive tumour-targeting mechanism of nanomedicines through the EPR effect offers low tumour-targeting efficiency, which is suboptimal for targeted tumour therapy. To address this problem, herein we report an active tumour-targeting strategy to design tumour-homing chimeric polypeptide-conjugated NIR-absorbing conjugated-polymer nanoparticles as a new class of drug nanocarriers for imaging-guided combination therapy of cancer.

F3 is the N-terminal fragment of human high-mobility group protein 2 (HMGN2) [24]. Through specific binding to nucleolin expressed on the membrane of tumour cells and tumour endothelial cells, F3 can be internalized into the targeted cells and translocated to the nucleus. Elastin-like polypeptides (ELPs) are a class of biopolymers composed of a VPGXG repeat unit derived from human tropoelastin, in which X can be any amino acid except proline [25]. ELPs have been used as a new class of biomaterials for drug delivery [26,27], due to their precise control of structure and properties at the gene level, biodegradability, and excellent biocompatibility [28-30]. In our previous work, F3 was genetically fused with an ELP appended with a cysteine-rich amino acid sequence (Gly-Gly-Cys)$_8$ (C8) to yield a tumour-homing chimeric polypeptide F3-ELP-C8 [31]. F3-ELP-C8 was chemoselectively conjugated with DOX at the site of C8 to form tumour-homing and pH-responsive F3-ELP-DOX nanoparticles for targeted chemotherapy of cancer.

In this study, F3 was genetically fused to the C-terminus of an ELP with a cysteine residue at the N-terminus (C-ELP) to form a tumour-homing chimeric polypeptide C-ELP-F3. C-ELP-F3 was chemoselectively conjugated to PPy nanoparticles via a facile thiol-maleimide coupling reaction to form ELP-F3-conjugated PPy nanoparticles (PPy-ELP-F3) (**Figure 1A**). PPy-ELP-F3 were explored as an active tumour-targeting drug carrier to load DOX through π-π stacking to yield DOX-loaded PPy-ELP-F3 (DOX/PPy-ELP-F3). DOX/PPy-ELP-F3 showed more cytotoxicity to cancer cells *in vitro* than both DOX/PPy-ELP without the tumour-homing function and free DOX, and more accumulation in tumours *in vivo*. More importantly, under the guidance of photoacoustic and photothermal imaging, a synergistic photothermal and chemical therapy in which tumours were completely abolished without detectable systemic toxicity was achieved by DOX/PPy-ELP-F3 rather than DOX/PPy-ELP (**Figure 1B**).

Results and discussion

Synthesis and characterization of DOX/PPy-ELP-F3 nanoparticles

ELP-F3 and C-ELP were overexpressed in *Escherichia coli* (*E. coli*) and subsequently purified by inverse transition cycling (ITC). Sodium dodecyl sulfate polyacrylamide gel electrophoresis (SDS-PAGE) showed that the molecular weights of C-ELP-F3 and C-ELP with high purity were ~16.9 kD and ~13.6 kD, respectively (**Figure S1**). Dynamic light scattering (DLS) showed that the phase transition temperatures (T_t) of C-ELP-F3 and C-ELP at a concentration of 25 μM in PBS were 44 °C and 32 °C, respectively (**Figure S2**). PPy nanoparticles (PPy) stabilized with PVA were synthesized via a one-step aqueous dispersion polymerization of pyrrole. The surface of PPy was modified with maleic anhydride (MA) to form PPy-MA, followed by chemoselective conjugation of C-ELP-F3 and C-ELP to form PPy-ELP-F3 and PPy-ELP, respectively (**Figure S3**). Subsequently, DOX was physically adsorbed onto the surfaces of PPy-ELP-F3 and PPy-ELP to yield DOX/PPy-ELP-F3 and DOX/PPy-ELP, respectively. Zeta potential measurements showed that the maleic anhydride modification of PPy made the surface of PPy more negatively charged (**Tabel S1**), as expected. In contrast, the C-ELP-F3 and C-ELP modifications made the zeta potential of PPy-MA less negative, due

to the positively charged characteristics of C-ELP-F3 and C-ELP. Subsequent DOX adsorption further made the zeta potential of PPy-ELP-F3 less negative, due to the positively charged characteristic of DOX. DLS showed that these surface modifications of PPy increased their size (**Figure 2A** and **Figure S4**). Transmission electron microscopy (TEM) revealed the uniform spherical morphology of DOX/PPy-ELP-F3 (46.71 ± 3.74 nm in diameter) and DOX/PPy-ELP (45.60 ± 4.05 nm in diameter) (**Figure 2B** and **Figure S5**). The absorption spectra of DOX/PPy-ELP-F3 and DOX/PPy-ELP showed an obvious new absorption shoulder peak at 480 nm that corresponded to the characteristic absorption of DOX, as compared with PPy-ELP-F3, PPy-ELP and PPy (**Figure 2C** and **Figure S6**), indicating the successful adsorption of DOX onto PPy-ELP-F3 and PPy-ELP. The phase transition behaviors of DOX/PPy-ELP-F3, DOX/PPy-ELP and PPy were examined by DLS (**Figure 2D** and **Figure S7**). PPy did not show any phase transition behavior;

in contrast, DOX/PPy-ELP-F3 and DOX/PPy-ELP showed evident phase transition behaviors with T_t of 65 °C and 50 °C at the same PPy concentration of 500 mg/L, respectively, indicating the success of the chemoselective conjugation of C-ELP-F3 and C-ELP to PPy. Next, the photothermal effect of DOX/PPy-ELP-F3 was investigated. As expected, the photothermal effect of DOX/PPy-ELP-F3 and DOX/PPy-ELP was enhanced by increasing the 808 nm laser power or the PPy concentration (**Figure 2E-F** and **Figure S8-9**). The photothermal transfer efficiency of DOX/PPy-ELP-F3 was 33.6%, similar to that of PPy (32.7%) (**Figure S10**). Furthermore, the photothermal effect of DOX/PPy-ELP-F3 and DOX/PPy-ELP could be used to accelerate the release of DOX from PPy-ELP-F3 and PPy-ELP, as indicated by the dramatic increases of DOX release at pH 7.4 and 5.5 upon laser irradiation at 2 h and 5 h (**Figure 2G** and **Figure S11**). Such kind of phenomenon was also observed in the literature [19, 32].
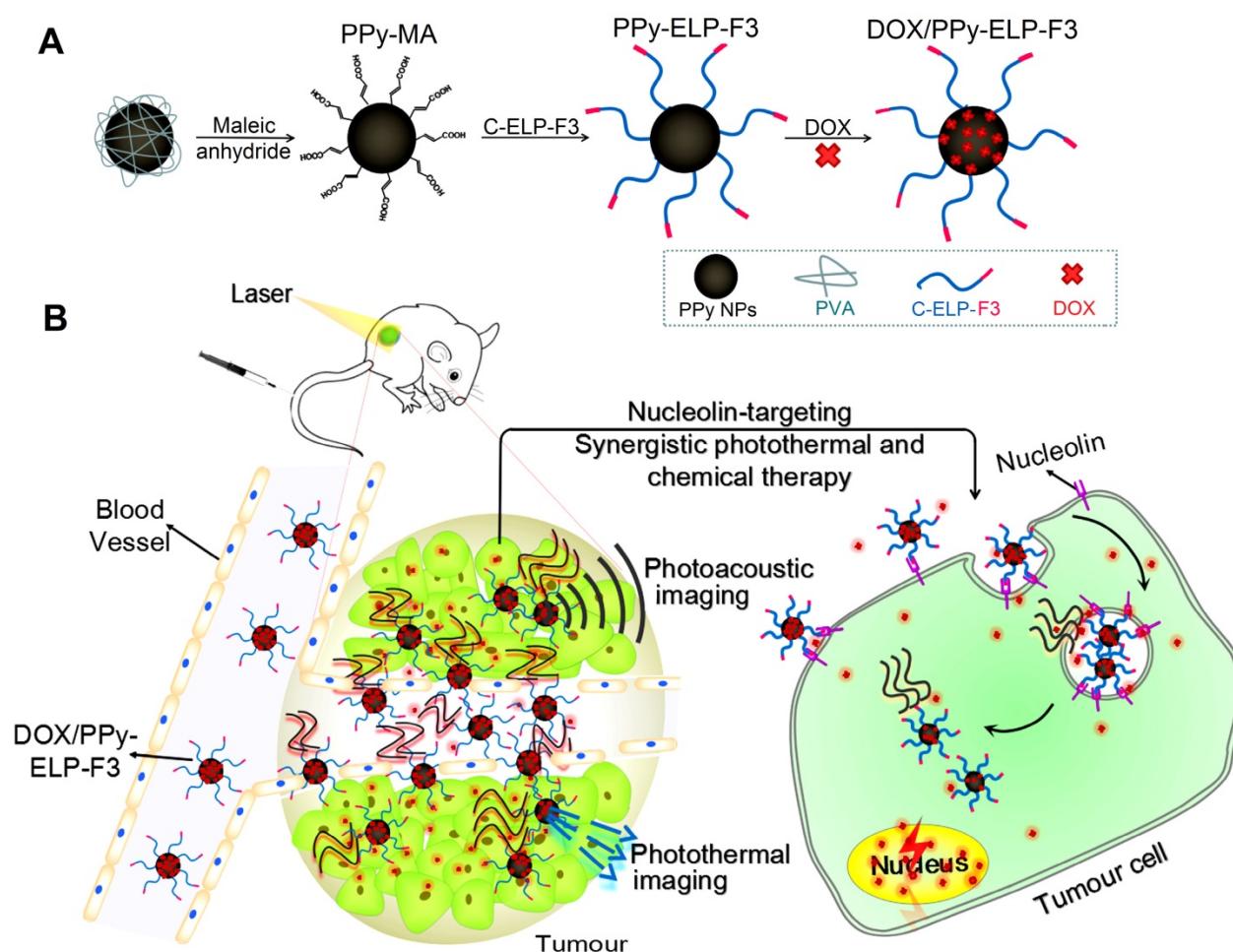
Figure 1. Synthesis of DOX/PPy-ELP-F3 nanoparticles for imaging-guided synergistic photothermal and chemical therapy of cancer. **(A)** Schematic illustration of the synthesis of DOX/PPy-ELP-F3 nanoparticles. **(B)** Schematic representation of photoacoustic and photothermal imaging-guided synergistic photothermal and chemical therapy enabled by DOX/PPy-ELP-F3 nanoparticles.
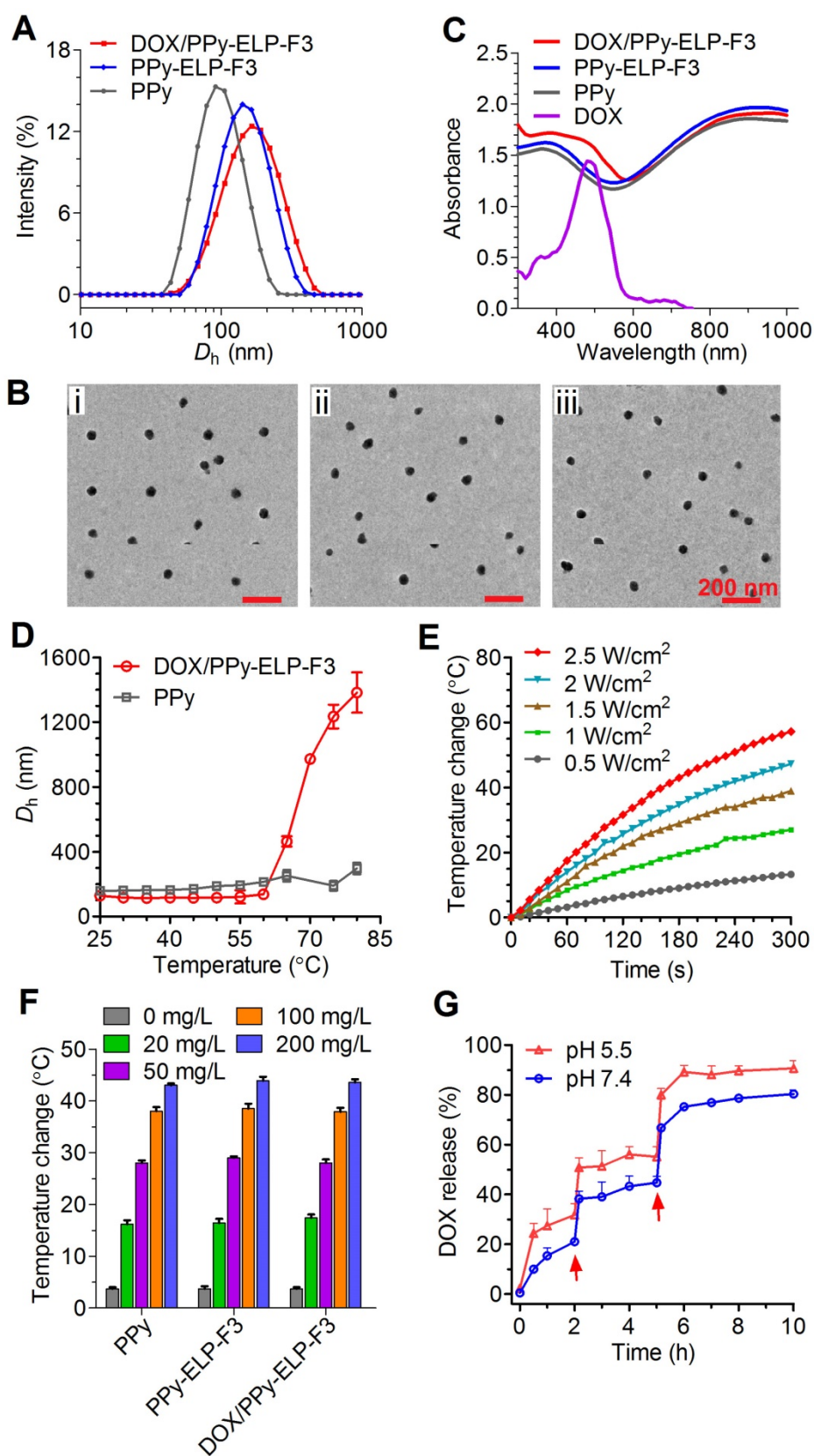
Figure 2. Physicochemical characterization of DOX/PPy-ELP-F3 nanoparticles. **(A)** The hydrodynamic diameters (D_h) of PPy, PPy-ELP-F3 and DOX/PPy-ELP-F3 determined by DLS. **(B)** The TEM images of PPy (i), PPy-ELP-F3 (ii) and DOX/PPy-ELP-F3 (iii) at 25 °C. **(C)** The absorption spectra of DOX, PPy, PPy-ELP-F3 and DOX/PPy-ELP-F3 at the same PPy concentration (200 mg/L) in PBS at 25 °C. **(D)** The temperature dependence of hydrodynamic diameter (D_h) of DOX/PPy-ELP-F3 or PPy at the same concentration of PPy (500 mg/L). **(E)** The temperatures of DOX/PPy-ELP-F3 solution (100 mg/L) exposed to laser irradiation (808 nm) for 5 min at different power densities. **(F)** The PPy concentration dependence of temperature of PPy, PPy-ELP-F3 or DOX/PPy-ELP-F3 solution exposed to laser irradiation (808 nm, 1.5 W/cm², 5 min). **(G)** NIR-triggered DOX release from DOX/PPy-ELP-F3 at different pH values. Arrows indicate the time points when NIR irradiation (808 nm, 1.0 W/cm²) was executed for 5 min. Error bars are based on standard deviations of triplicated samples.

Investigation of *in vitro* synergistic photothermal and chemical therapy

The chemical and photothermal cytotoxicity of DOX/PPy-ELP-F3 against C8161 melanoma cells was examined by MTS assay. DOX/PPy-ELP-F3 was more cytotoxic than free DOX (**Figure 3A**). PPy-ELP-F3 was not cytotoxic, but became cytotoxic under laser irradiation (**Figure 3B**). Laser irradiation did not enhance the cytotoxicity of free DOX, but made DOX/PPy-ELP-F3 more cytotoxic due to the synergistic photothermal and chemical effect of DOX/PPy-ELP-F3. Similarly, laser irradiation enhanced the cytotoxicity of DOX/PPy-ELP (**Figure S12**). However, DOX/PPy-ELP-F3 showed more cytotoxicity than DOX/PPy-ELP due to the active-targeting effect of F3 [31]. The combination index (C.I.) was calculated to be 0.18, which indicated the synergistic effect of DOX/PPy-ELP-F3 in chemotherapy and PTT [33]. The active-targeting effect was confirmed by cellular uptake experiments. Confocal laser scanning microscopy (CLSM) and fluorescence-activated cell sorting (FACS) analyses showed that more DOX was observed in cancer cells for DOX/PPy-ELP-F3 than for DOX/PPy-ELP (**Figure 2C-E** and **Figure S13-14**). Moreover, laser irradiation enhanced the cellular uptake of DOX/PPy-ELP-F3 and DOX/PPy-ELP. The synergistic photothermal and chemical effect of DOX/PPy-ELP-F3 was confirmed by fluorescence imaging of C8161 melanoma cells stained with propidium iodide (PI) to distinguish dead cells (red) from live ones (green) (**Figure 3F**). Without laser irradiation, cell death was not observed for the treatment with PPy-ELP-F3, but was observed for the treatment with DOX/PPy-ELP-F3. Laser irradiation induced cell death for the treatment with PPy-ELP-F3 and complete cell death for the treatment with DOX/PPy-ELP-F3. Similarly, a synergistic photothermal and chemical effect was observed for the treatment with DOX/PPy-ELP (**Figure S15**). Additionally, both PPy-ELP-F3 and PPy-ELP were non-toxic to normal cells (**Figure S16**). These results indicated that the synergistic photothermal and chemical effect of DOX/PPy-ELP-F3 could be used to kill cancer cells with high efficiency.

In vivo pharmacokinetics, biodistribution and imaging

Encouraged by the *in vitro* synergistic photothermal and chemical effect of DOX/PPy-ELP-F3, we further studied their *in vivo* synergistic photothermal and chemical effect. At first, we examined their *in vivo* pharmacokinetics in a mouse model (**Figure S17**). DOX/PPy-ELP-F3 and DOX/PPy-ELP had almost the same terminal half-life of 20.6 h, which was 3.9-fold longer than that (5.3 h) of free DOX (**Table S2**). The areas under the curves (AUCs) of DOX/PPy-ELP-F3 (40.2 μM/L×h) and DOX/PPy-ELP (42.4 μM/L×h) were 6.9- and 7.3-fold larger than that (5.8 μM/L×h) of free DOX, respectively. These results indicated that PPy-ELP-F3 and PPy-ELP as drug carriers significantly improved the *in vivo* pharmacokinetics of DOX. The distribution of DOX/PPy-ELP-F3 in major organs and tissues was further investigated at representative time points of 2 h, 9 h and 24 h after intravenous injection (**Figure 4A** and **Figure S18**). Particularly, both DOX/PPy-ELP-F3 and DOX/PPy-ELP showed the maximum DOX concentration in tumour tissue at 9 h, but the DOX concentration at 9 h of DOX/PPy-ELP-F3 (6.3% ID/g) was higher than that of DOX/PPy-ELP (4.8% ID/g), with significant difference (*P < 0.05) between them. These results were confirmed by photoacoustic imaging (**Figure 4B** and **Figure S19**) and infrared thermal imaging that were based on the photothermal effect of PPy (**Figure S20**). As expected, the maximum photoacoustic signal and temperature were detected at 9 h post intravenous injection of DOX/PPy-ELP-F3 or DOX/PPy-ELP, and the photoacoustic signal (3.27 × 10^4 dB) and temperature (57.1 ℃) at 9 h post injection of DOX/PPy-ELP-F3 was higher than those of DOX/PPy-ELP (2.72 × 10^4 dB and 53.2 ℃), respectively. Next, we studied the *in vivo* photothermal effect of DOX/PPy-ELP-F3 in a melanoma mouse model by using infrared thermal imaging at 9 h post intravenous injection. Laser irradiation increased the local temperatures of tumours of mice treated with DOX/PPy-ELP-F3, DOX/PPy-ELP, DOX, and saline by 22.7 ℃, 19.6 ℃, 5.9 ℃ and 5.5 ℃, respectively (**Figure 4C** and **Figure S21**), indicating the high photothermal efficiency of DOX/PPy-ELP-F3.

In vivo synergistic photothermal and chemical therapy

Under the guidance of infrared thermal imaging and photoacoustic imaging, the therapeutic efficacy of DOX/PPy-ELP-F3 was further studied in a melanoma mouse model. At first, the maximum tolerated dose (MTD) of DOX/PPy-ELP-F3 was investigated (**Figure S22**). The MTDs of DOX/PPy-ELP-F3, DOX/PPy-ELP and free DOX were determined to be 20, 20 and 10 mg DOX equivalent/kg body weight, respectively. Melanoma-bearing mice were intravenously injected with DOX/PPy-ELP-F3, DOX/PPy-ELP and free DOX at their MTDs. DOX plus laser treatment slightly inhibited tumour growth as compared with laser only treatment (**Figure 5A** and **Figure S23**).
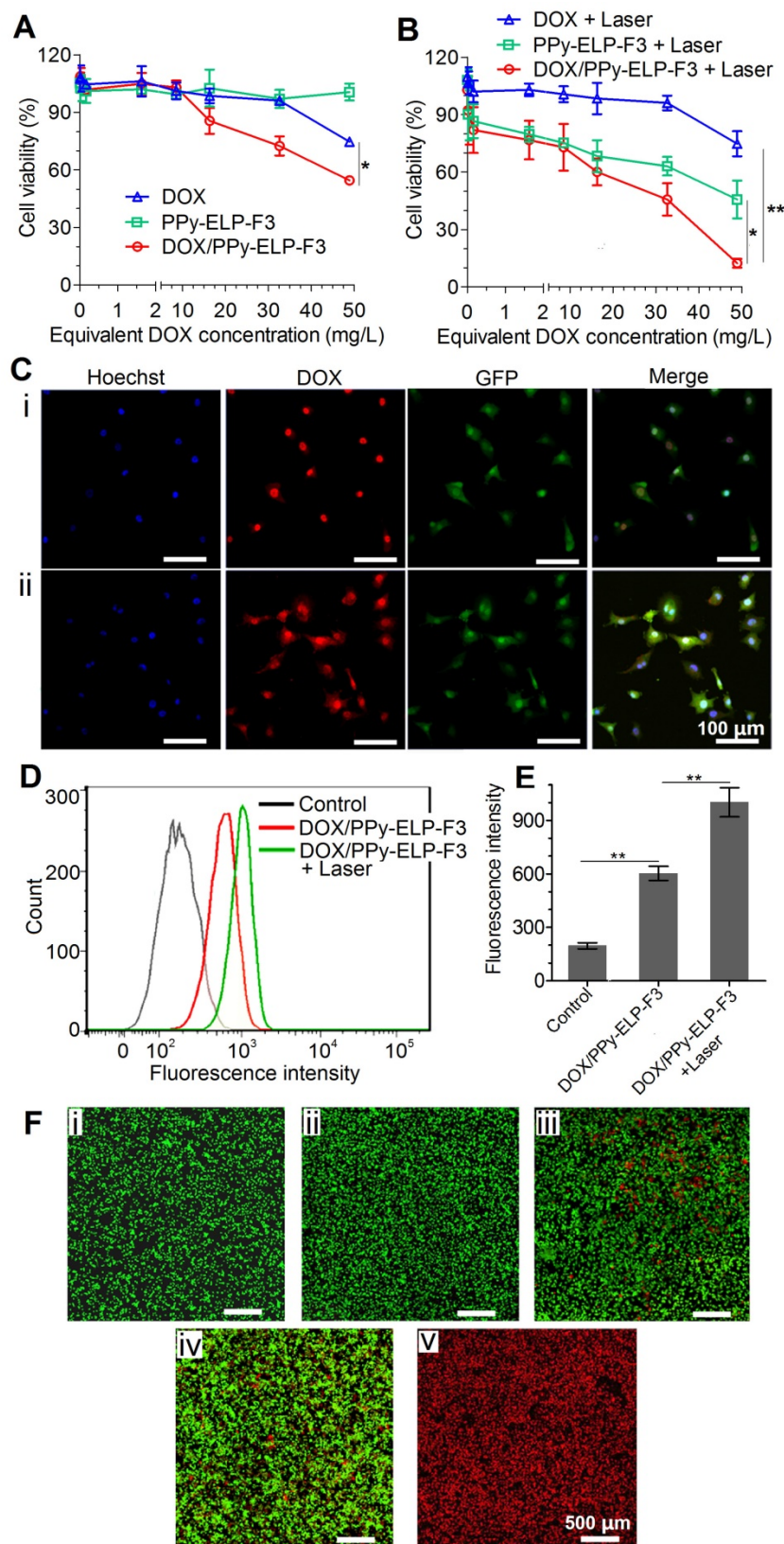
Figure 3. Chemical-photothermal cytotoxicity and endocytosis of DOX/PPy-ELP-F3 against C8161 melanoma cancer cells. **(A-B)** Cell viability of C8161 cells after incubation with different samples for 4 h (A), followed by NIR irradiation (808 nm, 2.5 W/cm², 3 min) (B). *$P < 0.05$, **$P < 0.01$, significant difference for DOX/PPy-ELP-F3 plus laser compared with DOX plus laser. Note: The concentration of PPy-ELP-F3 was equivalent to the PPy-ELP-F3 concentration of DOX/PPy-ELP-F3. The weight ratio of DOX to PPy-ELP-F3 was set to be 1:5. **(C)** Intracellular delivery of DOX into C8161 cells by DOX/PPy-ELP-F3 without (i) or with (ii) laser irradiation. The cell nucleus was stained with Hoechst 33324 in blue; the cell membrane is green (GFP); DOX/PPy-ELP-F3 are shown in red. **(D)** FACS analysis of C8161 cell uptake of DOX/PPy-ELP-F3 with or without laser irradiation. Laser irradiation: 808 nm, 1.0 W/cm², 2 min. **(E)** The mean fluorescence intensity of cells quantified from the FACS analysis. **$P < 0.01$, significant difference for DOX/PPy-ELP-F3 plus laser compared with other treatment groups. **(F)** Fluorescence imaging of C8161 cells treated with laser only (i), PPy-ELP-F3 only (ii), DOX/PPy-ELP-F3 only (iii), PPy-ELP-F3 plus laser (iv), or DOX/PPy-ELP-F3 plus laser (v). Laser irradiation: 808 nm, 2.5 W/cm², 3 min.
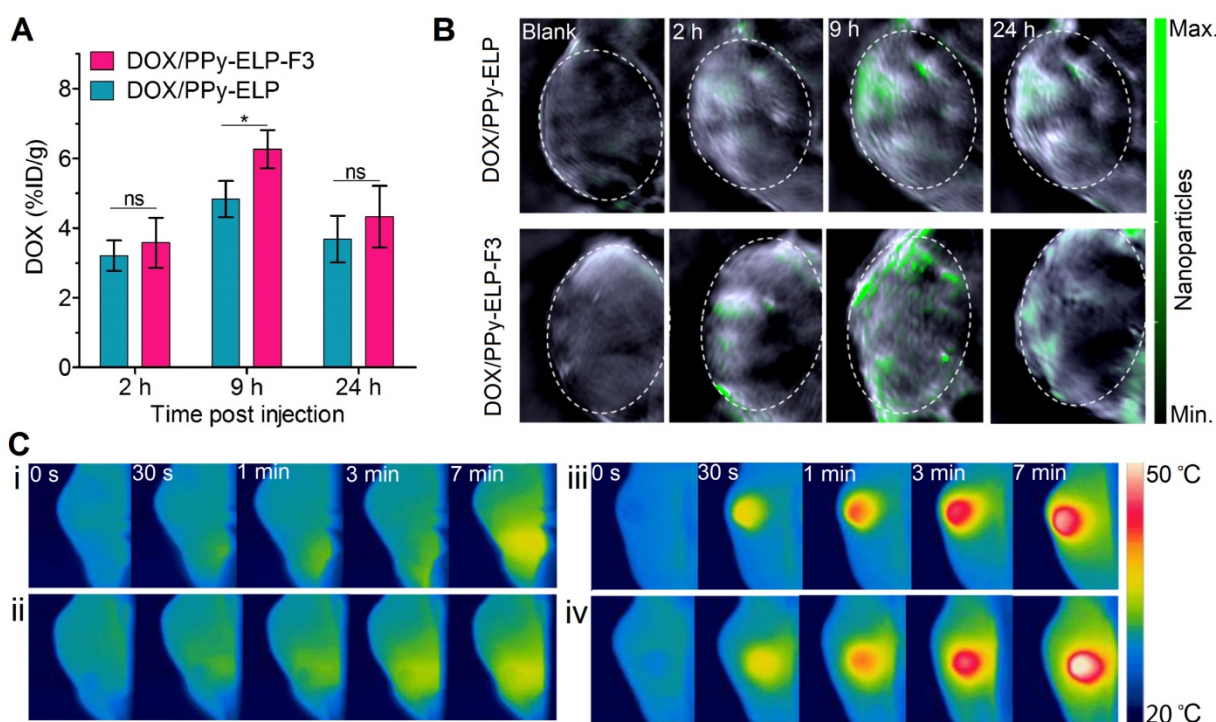
Figure 4. *In vivo* distribution and imaging of DOX/PPy-ELP-F3. **(A)** Biodistribution of DOX from DOX/PPy-ELP-F3 and DOX/PPy-ELP in tumours at 2 h, 9 h and 24 h post administration. Data are shown as mean ± standard deviation (n = 3). *$P < 0.05$: significant difference for DOX/PPy-ELP-F3 compared with DOX/PPy-ELP at 9 h post injection, ns: non-significant differences between nanoparticle groups at 2 h and 24 h post injection. **(B)** Photoacoustic images of tumor tissues before and after intravenous injection of DOX/PPy-ELP (1 mg PPy) and DOX/PPy-ELP-F3 (1 mg PPy). **(C)** IR thermal images of C8161 tumour-bearing mice exposed to an 808 nm laser (1.2 W/cm²) at 9 h after intravenous injection with saline (i), DOX (ii), DOX/PPy-ELP (iii) or DOX/PPy-ELP-F3 (iv).

DOX/PPy-ELP-F3 treatment showed better tumour growth inhibition than DOX plus laser treatment, indicating that PPy-ELP-F3 as a new drug carrier could enhance the antitumour efficacy of DOX. PPy-ELP-F3 plus laser treatment exhibited enhanced antitumour efficacy as compared with laser only treatment, indicating the effective photothermal effect of PPy-ELP-F3 in melanoma therapy. As a result, DOX/PPy-ELP-F3 plus laser treatment completely eradicated tumours without any recurrence due to the synergistic effect of chemotherapy and photothermal therapy. In contrast, DOX/PPy-ELP plus laser treatment could not completely abolish tumours due to the lack of tumour-targeting function. Correspondingly, no animal deaths were observed for DOX/PPy-ELP-F3 plus laser treatment (**Figure 5B**). The median survival times for DOX/PPy-ELP plus laser, PPy-ELP-F3 plus laser, DOX/PPy-ELP-F3, DOX plus laser, and laser only treatments were 35 days, 20.4 days, 18 days, 13.2 days and 12.6 days, respectively. The antitumour efficacy of DOX/ PPy-ELP-F3 with laser irradiation was confirmed by hematoxylin and eosin (H&E) staining of tumour tissue, in which severe damage of cancer cells was observed in the tumour of DOX/PPy-ELP-F3 plus laser treated group as compared to other treatment groups (**Figure 5C**). No damage to other important organs was observed for all treatment groups (**Figure S24**). No significant body weight loss was found for all treatment groups (**Figure S25**). Biochemistry and hematology analyses showed that DOX/PPy-ELP-F3 plus laser treatment did not cause significant toxicity to major organs and blood (**Figure S26** and **Table S3**). Taken together, these results indicated that DOX/ PPy-ELP-F3 in combination with laser irradiation could be used to treat melanoma with high efficiency without detectable side effects due to the synergy of photothermal therapy and chemotherapy. The synergy of photothermal and chemical effect of DOX/PPy-ELP-F3 could be ascribed to the enhanced cell uptake by photothermal effect.

Conclusions

This paper has reported an active tumour targeting strategy to design a new class of multi-functional nanomedicines such as DOX/PPy-ELP-F3 for photoacoustic and thermal imaging-guided synergistic photothermal and chemical therapy of cancer. These new nanomedicines exhibit intriguing attributes for cancer therapy. First, tumour-homing chimeric polypeptides can be various [31,34]; particularly, the tumour-homing moiety can be one of dozens of tumour-homing peptides [35]. Second, ELP-based tumour-homing chimeric polypeptides can be genetically engineered with precisely defined structures and functions.
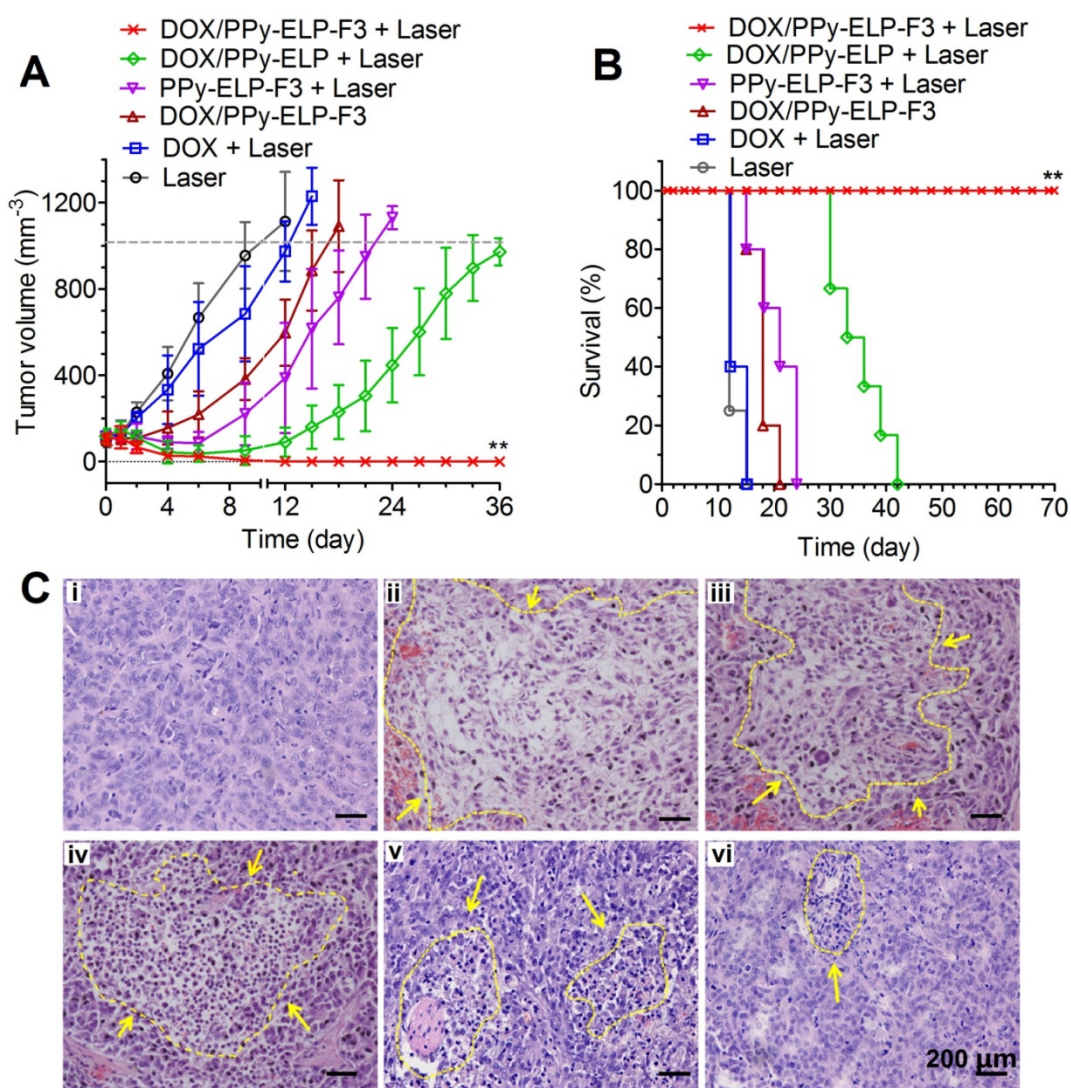
Figure 5. *In vivo* therapeutic efficacy after single intravenous injection of DOX/PPy-ELP-F3. **(A)** Tumour growth curves of C8161 tumour-bearing mice after different treatments. Error bars are based on standard deviations of 4-7 mice per group. **(B)** Survival curves of C8161 tumour mice after various treatments. *******P* < 0.01, significant difference for DOX/PPy-ELP-F3 plus laser compared with other treatment groups. **(C)** H&E staining of tumours collected at 2 days post different treatments: laser only (i), DOX/PPy-ELP-F3 plus laser (ii), DOX/PPy-ELP plus laser (iii), PPy-ELP-F3 plus laser (iv), DOX/PPy-ELP-F3 plus laser (v), DOX plus laser (vi).

Particularly, these polypeptides can be produced in *E. coli* and easily purified by a facile non-chromatographic method of ITC. They are biocompatible and biodegradable [28-31,35]. Third, these polypeptides can be chemoselectively conjugated to NIR-absorbing conjugated polymer nanoparticles to form a new class of multifunctional drug carriers. Fourth, a variety of drugs can be readily loaded onto the nanocarriers by physical and/or chemical interactions between the drugs and conjugated polymer nanoparticles. Fourth, the nanocarriers can significantly improve the pharmacokinetics, biodistribution and therapeutic effect of the drugs. Particularly, the photothermal effect of the nanocarriers can trigger the release of drugs and enable imaging-guided synergistic photothermal and chemical therapy of cancer in which tumours can be completely abolished. The tunable, well-defined, versatile, highly efficient characteristics of tumour-homing chimeric polypeptide-conjugated NIR-absorbing conjugated-polymer nanoparticles make them interesting as a new class of multifunctional drug carriers for imaging-guided combination therapy of cancer.

Methods

Materials

All chemical reagents were purchased from Sigma Aldrich. Molecular biology reagents were from New England Biolabs. Cell culture reagents and media were from Gibco. The metastatic human C8161 melanoma cell line expressed green fluorescent protein (GFP). The gene sequences of ELP (VGVPG) and F3 peptide (KDEPQRRSARLSAKPAPPKPEPKP KAPAKK) were synthesized by Sangon Biotech (Shanghai) Co., Ltd.

Construction and purification of C-ELP-F3

The ELP gene in a recombinant vector was constructed by recursive directional ligation by plasmid reconstruction (PRe-RDL) method [36]. In this method, a cysteine was genetically fused at the N-terminus of ELP, and F3 was genetically fused at the C-terminus of ELP.

The recombinant plasmid was transformed into *Escherichia coli* BL21 (DE3) competents (Invitrogen) and C-ELP-F3 was further purified by inverse transition cycling (ITC) method [37], as described in our previous paper [38]. The concentration of purified C-ELP-F3 was determined by absorbance at 280 nm. The purity was further determined on sodium dodecyl sulfate polyacrylamide gel electrophoresis (SDS-PAGE). Similarly, C-ELP was synthesized by the same method as above.

Synthesis of DOX/PPy-ELP-F3 nanoparticles

Polypyrrole nanoparticles (PPy) were prepared using poly(vinyl alcohol) (PVA, Mw: 9000-10000)/ FeCl$_3$ mixture and pyrrole monomer in distilled water [39]. 1.4 g PVA was dissolved in 20 mL distilled water, followed by addition of 0.23 mol FeCl$_3$·6H$_2$O. After stirring for 1 h at 4 °C, 2 mmol pyrrole monomer was added into the mixture with vigorous stirring for 4 h at 4 °C. The PPy were purified by centrifugation and dialysis against 0.1 M NaHCO$_3$ solution (pH 8.4) (dialysis bag: MWCO 100 kDa). Then 13.2 g MA in DMSO (20 mL) was dropped into 20 mL PPy (0.8 g/L) solution with stirring for 24 h. The PPy-MA were dialyzed against NaHCO$_3$ (0.1 M) and then PBS (10 mM, pH 7.4) (dialysis bag: MWCO 100 kDa).

PPy-MA were first allowed to react with C-ELP-F3. C-ELP-F3 solution was added to 10 mL PPy-MA (10 mg) in PBS to a final concentration of 20 μM, and stirred vigorously for 24 h. For loading of doxorubicin (DOX), 3 mg DOX in 300 μL DMSO was added to the mixture with stirring for another 7 h. DOX/PPy-ELP-F3 was collected by centrifugation (12500 rcf for 30 min, 15 °C) and re-dispersed in PBS for further use. The loading capacity was determined by the following equation:

$$\text{DOX loading capacity (mg/mg)} = (m_{[\text{initial DOX}]} - m_{[\text{DOX in supernatant}]}) / m_{[\text{PPy-ELP-F3}]}$$

In addition, PPy-ELP and DOX/PPy-ELP nanoparticles were synthesized by the same method as described above. As a result, for DOX/PPy-ELP-F3 and DOX/PPy-ELP nanoparticles, the loading capacity was 1 mg DOX /5 mg PPy.

Physicochemical characterization of DOX/PPy-ELP-F3

The hydrodynamic size and surface charge (zeta potential) were evaluated with a Nano Zeta Sizer (Malvern Instruments, Worcestershire, UK) at 25 °C. UV-vis spectra were recorded on a SpectraMax® M3 Microplate Reader (Molecular Devices) in concert with *Softmax Pro*. Particle size and surface morphology were observed by Hitichi-H-7650B transmission electron microscopy (TEM). To investigate the thermoresponsive behavior of DOX/PPy-ELP-F3, samples were allowed to incubate at different temperatures (from 25 °C to 80 °C) and analyzed by DLS, and hydrodynamic diameters (D_h) were monitored every 5 °C.

In vitro photothermal effect

1 mL sample in a disposable cuvette was exposed to an 808 nm laser at a power density of 1.5 W/cm^2. Temperature change was measured by a digital thermometer every 10 s. PBS was used as the control.

DOX release experiments

To evaluate *in vitro* DOX release from nanoparticles, DOX/PPy-ELP-F3 in dialysis bags was immersed in 50 mM PBS of pH 5.5 or pH 7.4 at 37 °C (dialysis bag: MWCO 100 kDa). The released DOX in the dialysate was collected and determined by absorbance at 480 nm (OD$_{480}$). For *in vitro* NIR-triggered DOX release, samples were exposed to laser irradiation for 5 min (808 nm, 1.0 W/cm^2) at the time points of 2 h and 5 h. After dialysis for another 3 min, the cumulative released DOX was collected immediately.

In vitro photothermal and chemical therapy

In vitro synergistic photothermal and chemical therapy was performed in a 35 mm plate with 2×10^5 C8161 cells, and PPy-ELP-F3 or DOX/PPy-ELP-F3 was added and incubated for 4 h. Then, a NIR laser (808 nm, 2.5 W/cm^2) was used to irradiate cells for 3 min, followed by propidium iodide (PI) staining. Cell viability was observed using a laser scanning confocal microscope (LSM780, Zeiss), where living cells had green fluorescence from GFP and dead ones stained by PI had red fluorescence. Other groups were operated in the same method as described above.

For cell proliferation assay, C8161 cells in 96-well plates (4000 cells/well) were incubated with DOX, PPy-ELP-F3 and DOX/PPy-ELP-F3 in concentration gradients for 4 h. the 808 nm laser irradiation was 2.5 W/cm^2 for 3 min. Cytotoxicity was determined by MTS assay.

Cell endocytosis of DOX/PPy-ELP-F3

C8161 cells were seeded in a confocal dish and incubated with DOX/PPy-ELP-F3 (450 μg) or DOX/PPy-ELP (450 μg) at 37 °C for 30 min. Then, cells were washed, immediately fixed in 4% para-

formaldehyde and stained by Hoechst 33324 (nucleus dye). Cell endocytosis assay was determined using a laser scanning confocal microscope (LSM780, Zeiss). For quantitative analysis, cells were collected and analyzed by fluorescence-activated cell sorting (FACS) method by FACS Aria II (BD, 488 nm). In NIR-stimulated endocytosis experiments, an 808 nm laser (1.0 W/cm², 2 min) was applied at 15 min post incubation.

Biocompatibility study of PPy-ELP-F3

Murine fibroblasts L929 cells, human mammary epithelial MCF-10A cells and human microvascular endothelial cells (HMECs) were used for biocompatibility assay. Briefly, cells were plated in a 96-well plate at a density of 5000 cells/well, and then fresh medium containing PPy-ELP-F3 at final concentrations of 0/100/200/300/600/800 mg/L was added. After 48 h, cell viability was determined by standard MTS assay as described above.

Animals and tumour-bearing models

Female BALB/c nude mice were obtained from Vital River Laboratories (Beijing, China), and female BALB/c mice were from AniKeeper (Beijing, China). All mice were raised in the animal research facility of Tsinghua University. The Laboratory Animal Facility at the Tsinghua University was accredited by AAA LAC (Association for Assessment and Accreditation of Laboratory Animal Care International), and all animal use protocols used in this study were approved by the Institutional Animal Care and Use Committee (IACUC). For building tumour-bearing models, female BALB/c nude mice 6 weeks of age were subcutaneously inoculated with a C8161 cells suspension (2×10^6) on the back. When the tumours reached a size of 100-120 mm³, C8161 tumour-bearing mice were available for further use.

Photoacoustic and photothermal imaging

For photoacoustic imaging, C8161 tumour-bearing mice were intravenously injected with 1 mg DOX/PPy-ELP-F3 or DOX/PPy-ELP. After 2 h, 9 h and 24 h, mice were anesthetized and imaged by a MSOT inVision 512-echo system (iTheraMedical, German) equipped with a 5 MHz, 128-element linear array transducer.

To visually determine the photothermal effect of nanoparticles on tumours, C8161 tumour-bearing mice were injected with saline, DOX, DOX/PPy-ELP and DOX/PPy-ELP-F3 (equivalent 2 mg PPy and 0.4 mg DOX) via the tail vein. After 9 h, mice were anesthetized and exposed to a 808 nm laser (1.2 W/cm², 7 min). During the irradiation, mice were imaged with a GF300 infrared camera (FLIR) to record the tumour local temperature change.

Maximum tolerated dose (MTD)

27 female Balb/c nude mice (6 weeks old) were divided into 9 groups, corresponding to DOX (5, 10, 15 mg/kg body weight), DOX/PPy-ELP (15, 20, 30 mg DOX equivalent/kg body weight) and DOX/PPy-ELP-F3 (15, 20, 30 mg DOX equivalent/kg body weight), respectively. Mice were intravenously injected with these drugs, and weighed every two days for two weeks. MTD was defined as the highest dose that did not cause more than 10% weight loss.

In vivo photothermal and chemical therapy

32 mice with C8161 tumour (100-120 mm³) on the back were randomly assigned to six groups, which were DOX/PPy-ELP-F3 with laser irradiation (n = 7), DOX/PPy-ELP with laser irradiation (n = 6), PPy-ELP-F3 with laser irradiation (n = 5), DOX with laser irradiation (n = 5), DOX/PPy-ELP-F3 only (n = 5) and laser irradiation only (n = 4). Mice from the "DOX with laser irradiation" group were injected with DOX at the MTD of 10 mg/kg body weight. Mice from other groups were intravenously injected with nanoparticles at the MTDs of 20 mg DOX equivalent/kg body weight and 2 mg PPy. At 9 h post injection, anesthetized mice were exposed to laser irradiation (808 nm, 1.2 W/cm²) for 7 min. Then, their tumour sizes and body weights were recorded every three days. The mice with tumour sizes over 1000 mm³ or more than 15% weight loss were executed.

Plasma pharmacokinetics analysis.

For pharmacokinetic study, female BALB/c mice were intravenously injected with DOX/PPy-ELP-F3, DOX/PPy-ELP and DOX at an equivalent dose of 5 mg DOX/kg body weight through the tail vein. At 1/5/15/30 min and 1/2/4/8/24/48 h post injection, blood samples were collected to obtain plasma. DOX in 10 µL plasma was extracted by 190 µL of acidified isopropanol (0.075 M HCl, 10% water) at -20 °C. DOX in the supernatant was measured by fluorescence (Ex: 488 nm, Em: 590 nm). The quantity was calculated from a linear standard curve of DOX concentrations from 0.001 µM to 10 µM. Each group had three parallel experiments. Plasma from a drug-free mouse was used as the background.

Histology analysis and blood analysis

Hematoxylin-eosin (H&E) staining was used to assess the damage to tumours and organs. Tumours from mice on the 2nd day post treatment were collected. Hearts, livers, spleens, lungs and kidneys were collected on the 12th day post treatment. The obtained tumours and organs were used for H&E staining assay and observed under an inverted microscope (Eclipse 90i, Nikon, Japan).

For standard serum biochemistry analysis, 80 µL of blood samples from mice on the 12th day post treatment with "DOX/PPy-ELP-F3 plus laser irradiation" were collected. To analyze the clinical biochemistry parameters, 300 µL of blood samples were collected retro-orbitally to collect plasma. All blood assays were operated at Tsinghua Hospital. Blood samples from mice treated with "PPy-ELP-F3 plus irradiation" and normal mice were used as controls. Each group had three parallel experiments.

Statistical analysis

All quantitative data are shown as mean ± standard deviation from 3 separate experiments except *in vivo* therapy (n = 4-7). All data were analyzed by two-tailed, unpaired Student's *t*-test. Differences between groups are shown as follows: "ns", $P > 0.05$ (not significant); *, $P < 0.05$ (significant); **, $P < 0.01$ (significant).

Abbreviations

DOX: doxorubicin; NIR: near infrared region; PTT: photothermal therapy; PAI: photoacoustic imaging; PPy: polypyrrole; PVA: poly(vinyl alcohol); ELP: elastin-like polypeptide; MA: maleic anhydride; EPR: enhanced permeability and retention; HMGN2: human high-mobility group protein 2; ITC: inverse transition cycling; T_t: phase transition temperature; DLS: dynamic light scattering; D_h: hydrodynamic diameter; R_h: hydrodynamic radius; TEM: transmission electron microscopy; C.I.: combination index; PRe-RDL: recursive directional ligation by plasmid reconstruction; MTD: maximum tolerated dose; SDS-PAGE: sodium dodecyl sulfate polyacrylamide gel electrophoresis.

Supplementary Material

Supplementary figures and tables show data for SDS-PAGE analyses and phase transition behaviors of C-ELP-F3 and C-ELP, absorption curves and phase transition behaviors of DOX/PPy-ELP, TEM analysis of DOX/PPy-ELP, heating curves and photothermal efficiency of nanoparticles, DOX release from DOX/PPy-ELP, cell experiments of DOX/PPy-ELP, *in vitro* biocompatibility and *in vivo* distribution of nanoparticles, maximum tolerated dose, and side effects of nanoparticles.
http://www.thno.org/v08p2634s1.pdf

Acknowledgements

Competing Interests

The authors have declared that no competing interest exists.

References

[1] Weissleder R. A clearer vision for in vivo imaging. Nat Biotechnol 2001; 19: 316-317.
[2] Hirsch LR, Stafford RJ, Bankson JA, Sershen SR, Rivera B, Price RE, et al. Nanoshell-mediated near-infrared thermal therapy of tumors under magnetic resonance guidance. Proc Natl Acad Sci U S A 2003; 100: 13549-13554.
[3] Huang X, El-Sayed IH, Qian W, El-Sayed MA. Cancer cell imaging and photothermal therapy in the near-infrared region by using gold nanorods. J Am Chem Soc 2006; 128: 2115-2120.
[4] Boisselier E, Astruc D. Gold nanoparticles in nanomedicine: preparations, imaging, diagnostics, therapies and toxicity. Chem Soc Rev 2009; 38: 1759-1782.
[5] Jain PK, Huang X, El-Sayed IH, El-Sayed MA. Noble metals on the nanoscale: optical and photothermal properties and some applications in imaging, sensing, biology, and medicine. Acc Chem Res 2008; 41: 1578-1586.
[6] Liu Y, Guo Q, Zhu X, Feng W, Wang L, Ma L, et al. Optimization of prussian blue coated NaDyF4:x%Lu nanocomposites for multifunctional imaging-guided photothermal therapy. Adv Funct Mater 2016; 26: 5120-5130.
[7] Zhu X, Feng W, Chang J, Tan Y, Li J, Chen M, et al. Temperature-feedback upconversion nanocomposite for accurate photothermal therapy at facile temperature. Nat Commun 2016; 7: 10437.
[8] Liu Y, Fan H, Guo Q, Jiang A, Du X, Zhou J. Ultra-small pH-responsive Nd-doped NaDyF$_4$ nanoagents for enhanced cancer theranostic by in situ aggregation. Theranostics 2017; 7: 4217-4228.
[9] Xu L, Cheng L, Wang C, Peng R, Liu Z. Conjugated polymers for photothermal therapy of cancer. Polym Chem 2014; 5: 1573-1580.
[10] Song X, Chen Q, Liu Z. Recent advances in the development of organic photothermal nano-agents. Nano Res 2015; 8: 340-354.
[11] Yang K, Xu H, Cheng L, Sun C, Wang J, Liu Z. In vitro and in vivo near-Infrared photothermal therapy of cancer using polypyrrole organic nanoparticles. Adv Mater 2012; 24: 5586-5592.
[12] Chen M, Fang X, Tang S, Zheng N. Polypyrrole Nanoparticles for high-performance in vivo near-infrared photothermal cancer therapy. Chem Commun 2012; 48: 8934-8936.
[13] Zha Z, Yue X, Ren Q, Dai Z. Uniform polypyrrole nanoparticles with high photothermal conversion efficiency for photothermal ablation of cancer cells. Adv Mater 2013; 25: 777-782.
[14] Wang X, Li H, Liu X, Tian Y, Guo H, Jiang T, et al. Enhanced photothermal therapy of biomimetic polypyrrole nanoparticles through improving blood flow perfusion. Biomaterials 2017; 143: 130-141.
[15] Liang X, Li Y, Li X, Jing L, Deng Z, Yue X, et al. PEGylated polypyrrole nanoparticles conjugating gadolinium chelates for dual-modal MRI/photoacoustic imaging guided photothermal therapy of cancer. Adv Funct Mater 2015; 25: 1451-1462.
[16] Yang J, Choi J, Bang D, Kim E, Lim EK, Park H, et al. Convertible organic nanoparticles for near-infrared photothermal ablation of cancer cells. Angew Chem Int Ed Engl 2011; 123: 461-464.
[17] Cheng L, Yang K, Chen Q, Liu Z. Organic stealth nanoparticles for highly effective in vivo near-infrared photothermal therapy of cancer. ACS Nano 2012; 6: 5605-5613.
[18] Gong H, Cheng L, Xiang J, Xu H, Feng L, Shi X, et al. Near-infrared absorbing polymeric nanoparticles as a versatile drug carrier for cancer combination therapy. Adv Funct Mater 2013; 23: 6059-6067.
[19] Wang C, Xu H, Liang C, Liu Y, Li Z, Yang G, et al. Iron oxide@polypyrrole nanoparticlesas a multifunctional drug carrier for remotely controlled cancer therapy with synergistic antitumor effect. ACS Nano 2013; 7: 6782-6795.
[20] Xue F, Shi M, Yan Y, Yang H, Zhou Z, Yang S. Iridium complex loaded polypyrrole nanoparticles for NIR laser induced photothermal effect and generation of singlet oxygen. RSC Adv 2016; 6: 15509-15512.
[21] Song X, Liang C, Feng L, Yang K, Liu Z. Iodine-131-labeled, transferrin-capped polypyrrole nanoparticles for tumor-targeted synergistic photothermal-radioisotope therapy. Biomater Sci 2017; 5: 1828-1835.
[22] Liu Y, Li L, Guo Q, Wang L, Liu D, Wei Z, et al. Novel Cs-based upconversion nanoparticles as dual-modal CT and UCL imaging agents for chemo-photothermal synergistic therapy. Theranostics 2016; 6: 1491-1505.
[23] Yang G, Xu L, Chao Y, Xu J, Sun X, Wu Y, et al. Hollow MnO$_2$ as a tumor-microenvironment responsive biodegradable nano-platform for combination therapy favoring antitumor immune responses. Nat Commun 2017; 8: 902-915.
[24] Porkka K, Laakkonen P, Hoffman JA, Bernasconi M, Ruoslahti E. A fragment of the HMGN2 protein homes to the nuclei of tumor cells and tumor endothelial cells in vivo. Proc Natl Acad Sci U S A 2002; 99: 7444-7449.

[25] Urry DW. Physical chemistry of biological free energy transduction as demonstrated by elastic protein-based polymers. J Phys Chem B 1997; 101: 11007-11028.

[26] Dreher MR, Raucher D, Balu N, Colvin OM, Ludeman SM, Chilkoti A. Evaluation of an elastin-like polypeptide-doxorubicin conjugate for cancer therapy. J Control Release 2003; 91: 31-43.

[27] MacKay JA, Chen MN, McDaniel JR, Liu WG, Simnick AJ, Chilkoti A. Self-assembling chimeric polypeptide-doxorubicin conjugate nanoparticles that abolish tumors after a single injection. Nat Mater 2009; 8: 993-999.

[28] Megeed Z, Cappello J, Ghandehari H. Genetically engineered silk-elastinlike protein polymers for controlled drug delivery. Adv Drug Deliv Rev 2002, 54: 1075-1091.

[29] Urry DW, Parker TM, Reid MC, Gowda DC. Biocompatibility of the bioelastic materials, poly(GVGVP) and its γ-irradiation cross-linked matrix: summary of generic biological test results. J Bioact Compat Polym 1991; 6: 263-281.

[30] Liu WE, Dreher MR, Furgeson DY, Peixoto KV, Yuan H, Zalutsky MR, et al. Tumor accumulation, degradation and pharmacokinetics of elastin-like polypeptides in nude mice. J Control Release 2006; 116: 170-178.

[31] Hu J, Xie L, Zhao W, Sun M, Liu X, Gao W. Design of tumor-homing and pH-responsive polypeptide-doxorubicin nanoparticles with enhanced anticancer efficacy and reduced side effects. Chem Commun 2015; 51: 11405-11408.

[32] Xing R, Bhirde A A, Wang S, Sun X, Liu G, Hou Y, et al. Hollow iron oxide nanoparticles as multidrug resistant drug delivery and imaging vehicles. Nano Res 2013; 6: 1-9.

[33] Zhao L, Wientjes MG, Au J L-S. Evaluation of combination chemotherapy: integration of nonlinear regression, curve shift, isobologram, and combination index analyses. Clin Cancer Res 2004; 10: 7994-8004.

[34] Wang Z, He Q, Zhao W, Luo J, Gao W. Tumor-homing, pH- and ultrasound-responsive polypeptide-doxorubicin nanoconjugates overcome doxorubicin resistance in cancer therapy. J Control Release 2017; 264: 66-75.

[35] Laakkonen P, Vuorinen K. Homing peptides as targeted delivery vehicles. Integr Biol 2010; 2: 326-337.

[36] McDaniel JR, MacKay JA, Quiroz FG, Chilkoti A. Recursive directional ligation by plasmid reconstruction allows rapid and seamless cloning of oligomeric genes. Biomacromolecules 2010; 11: 944-952.

[37] MacKay JA, Chen M, McDaniel JR, Liu W, Simnick AJ, Chilkoti A. Self-assembling chimeric polypeptide-doxorubicin conjugate nanoparticles that abolish tumours after a single injection. Nat Mater 2009; 8: 993-999.

[38] Sun M, Peng D, Hao H, Hu J, Wang D, Wang K, et al. Thermally triggered in situ assembly of gold nanoparticles for cancer multimodal imaging and photothermal therapy. ACS Appl Mater Interfaces 2017; 9: 10453-10460.

[39] Hong J Y, Yoon H, Jang J. Kinetic study of the formation of polypyrrole nanoparticles in water-soluble polymer/metal cation systems: a light-scattering analysis. Small 2010; 6: 679-686.